Species Correlation Measurements in Turbulent Flare Plumes: Considerations for Field Measurements

Scott P. Seymour, Matthew R. Johnson

Mechanical & Aerospace Engineering, Carleton University, Ottawa, K1S 5B6, Canada

5   *Correspondence to*: Matthew R. Johnson (matthew.johnson@carleton.com)

Abstract

Field measurement of flare emissions in turbulent flare plumes is an important and complex challenge. The simplest approaches necessarily assume that combustion species are spatially and/or temporally correlated in the plume, such that simple species ratios can be used to close a carbon balance to calculate species emission rates (*i.e.* emission factors) and flare

10   conversion efficiency. This study examines the veracity of this assumption and the associated implications for measurement uncertainty. A novel tunable diode laser absorption spectroscopy (TDLAS) system is used to measure the correlation between H_2O and black carbon (BC) volume fractions in the plumes of a vertical, turbulent, non-premixed, buoyancy-driven lab-scale gas flare. Experiments reveal that instantaneous, path-averaged concentrations of BC and H_2O can vary independently and are not necessarily well-correlated over short time intervals. The scatter in the BC/H_2O ratio along a path through the plume

15   was well beyond that which could be attributed to measurement uncertainty and was asymmetrically distributed about the mean. Consistent with previous field observations, this positive skewness toward higher BC/H_2O ratios implies short, localized, and infrequent bursts of high BC production, that are not well-correlated with H_2O. This demonstrates that the common assumption of fixed species ratios is not universally valid, and measurements based on limited samples, short sampling times, and/or limited spatial coverage of the plume could be subject to potentially large added uncertainty. For BC

20   emission measurements, the positive skewness of the BC/H_2O ratio also suggests that results from small numbers of samples are more likely to be biased low. However, a bootstrap analysis of the results shows how these issues should be easily avoidable with sufficient sample size and provides initial guidance for creating sampling protocols for future field measurements using analogous path-averaged techniques.

1   Introduction

25   Flaring in the upstream oil and gas industry (UOG) is a process used to destroy unwanted combustible gas, typically in buoyancy-driven, turbulent diffusion flames atop vertical stacks or in refractory-lined pits that are open to atmosphere. In 2019, global gas flaring volumes were estimated to be 150 billion m^3, up 3% from 2018, reaching levels not seen since 2009 (World Bank, 2020). Flaring is preferable to venting since the 20/100-year global warming potential (GWP) of methane, a common constituent of flare gas, is 96/34 times higher than the CO_2 produced by flaring (Gasser et al., 2017). However,

Atmospheric
Measurement
Techniques

Open Access

EGU

Discussions

30   flaring can also produce unwanted pollutants such as soot (primarily black carbon, which has its own important climate
impacts), CO, oxides of nitrogen (NOx), volatile organic compounds (VOCs), and uncombusted flare gases.

Of the pollutants produced by gas flaring, black carbon (BC; the carbonaceous, strongly light-absorbing component of soot)
has been suggested as the second most important atmospheric pollutant for climate forcing following CO_2 (*e.g.* Bond et al.,
35   2013; Jacobson, 2010; Ramanathan and Carmichael, 2008). Atmospheric BC directly warms the atmosphere as it is a strong
absorber of both in- and out-going radiation at all wavelengths (U.S. EPA, 2012). BC that is deposited onto Arctic snow and
ice has the additional effect of decreasing surface albedo (*i.e.* reflectance) and accelerating ice melting (Flanner, 2013; Sand
et al., 2016). Black carbon has a relatively short atmospheric lifetime (typically between 4-12 days, *e.g.* Cape et al., 2012) and
represents a unique mitigation opportunity to obtain near-term climatic benefits.

40

Field measurements of black carbon, and other pollutant emissions, from gas flaring in the upstream oil and gas industry are
limited. The lack of direct measurements is due to the difficulties in quantifying emissions in a turbulent, inhomogeneous,
and unconfined plume which freely entrains air as it evolves downstream. Field measurements generally fall into two
categories, intrusive (extractive) or non-intrusive (remote) sampling. Both measurement types tend to characterize flare
45   performance in broad terms such as pollutant emission factors (EFs), carbon conversion efficiency (CCE) also referred to as
"combustion efficiency" (CE), or destruction removal efficiency (DRE). These performance metrics are infrequently measured
and often applied to a large number of flares throughout the industry. It is therefore critical to obtain accurate estimates of
flare performance from field measurements. Uncertainties in global pollutant emission inventories stemming from
uncertainties in the few available measurements can have significant impact on climate modeling studies (Klimont et al., 2017;
50   Winiger et al., 2019; Zhao et al., 2011).

Extractive sampling techniques use an aspirated sampling system to pull gas samples into an instrument suite capable of
measuring the constituent species (sometimes simply CO_2, black carbon, and methane). The relative species concentrations
are then used to close a molar- or mass-balance of carbon to determine the desired flare performance metrics (*e.g.* Gvakharia
55   et al., 2017; Herndon et al., 2012; Pohl et al., 1986; Strosher, 2000; Weyant et al., 2016). Non-intrusive techniques typically
employ Fourier Transform Infrared Spectroscopy (FTIR, both active and passive) to measure column concentrations of each
species along a line-of-sight (LOS) through the plume (*e.g.* Blackwood, 2000; Wormhoudt et al., 2012). The relative column
concentrations of combustion species are similarly used to close a carbon balance. Critically, these techniques all rely on the
assumption that the species in these instantaneous measurements are well-mixed, and therefore well-correlated, in the plume.
60   Phrased in another way, these techniques assume that a ratio of two combustion-derived species is relatively constant spatially
and temporally within the plume. The veracity of this assumption is a necessary condition to obtaining representative flare
performance metrics. If, for example, concentrations of carbon species are weakly or perhaps inversely correlated in time
and/or space (*i.e.* a ratio of these species is not constant) within the turbulent plume, then instantaneous measurements using

the above approaches would be prone to error. Although it is possible that local variations in combustion efficiency or pollutant

65   emission may be averaged out in some of the available field measurement techniques, the number of required measurements is uncertain, and to date there has not been study attempting to directly inspect this potential issue.

This paper presents a first investigation of the instantaneous correlation of combustion product species in turbulent flare plumes. A unique measurement system was designed to measure instantaneous, path-averaged species correlations of black

70   carbon and H_2O concentrations in vertical flare plumes to understand if variations in relative species concentrations, and therefore variations in species ratios, are present. The results of these experiments provide insight into how these variations could affect field measurement techniques that assume constant combustion species ratios (*i.e.* well-correlated species). Further data analysis highlights potential implications for current field measurement approaches that should be considered when designing future measurement campaigns.

75   ## 2   Experimental Setup

2.1   Carleton University Flare Facility (CUFF)

Experiments were conducted at the Carleton University Flare Facility (CUFF) where custom gas mixtures characteristic of the upstream oil and gas industry can be flared. The facility is shown in schematic in Fig. 1, and has been previously discussed in Conrad and Johnson (2019). Custom combinations of C1-C4 alkanes, C2 and C3 alkenes, CO_2, and N_2 from pressurized gas

80   cylinders and evaporated C5-C7 alkanes from a controlled evaporative mixer (CEM) were combined and sent to a vertical flare nozzle to be combusted. The gas and liquid constituents were metered using thermal mass flow controllers and Coriolis mass flow controllers, respectively.

The gas mixtures were sent to a vertical flare nozzle (with selectable internal diameters of 25.4 mm, 50.8 mm, and 76.2 mm)

85   and combusted in a turbulent, buoyancy-driven, non-premixed flame. Experiments considered flare gas compositions, summarized in Table 1, characteristic of flaring in the Bakken oil region of North Dakota and in Ecuador as well as reference cases of pure methane and hydrogen. Prior to each experiment, the flare was run for up to 20 minutes to ensure the burner nozzle had reached a steady temperature.

90   A three-axis translating traverse system was outfitted with a square-channel semi-circular "hoop" that was positioned above the vertical flame. The hoop was manufactured from Invar, a nickel-iron alloy with a coefficient of thermal expansion of approximately 1.2×10^{-6} K^{-1} (roughly an order of magnitude less than stainless steel), which allowed rigid and stable mounting of the launch and collection optics of the black carbon and H_2O measurement system. The 1.5-m long optical measurement path was centered over the burner and positioned 2 m above the burner exit plane. Fiber optic cables and detector signal cables

95   were run from launch and collection optics to the laser driving and computer hardware systems located remotely as shown in
Fig. 1. This arrangement permitted the temperature-sensitive laser driving systems to be positioned well away from the flame.

2.2 Optical System

Figure 2 shows a schematic of the optical measurement system. Two distributed feedback (DFB) lasers at nominal wavelengths
of 1428 nm and 1654 nm from NTT Electronics were used for H_2O vapour and black carbon (BC) detection, respectively.

100   H_2O volume fraction was measured using tunable diode laser absorption spectroscopy (TDLAS) and BC volume fraction was
simultaneously measured via line-of-sight attenuation (LOSA). The radiation generated by each laser was fiber-coupled and
sent through separate single-mode fiber networks which included taps for wavelength references (fiber ring resonators), gas
reference cells, and laser power references. All reference components were housed in an enclosure thermally-stabilized by a
thermoelectric heater/cooler unit to prevent reference signal drift. Each laser was mounted in an ILX laser mount (LMD-4984)

105   and controlled by Stanford Research Systems (SRS) laser diode controller (LDC500). Light from each network was coupled
into a single fiber using a wavelength division multiplexer (WDM, WDM-12N-111-1428/1650 from Oz Optics) with optical
circulators (6015-3-APC, Thorlabs) to prevent light leakage between the two fiber networks. The combined wavelengths were
then sent in a single fiber to an open path beam collimator located on the optical hoop that launched the light through the flare
plume towards the collection optics 1.5 m away. This arrangement ensured that the H_2O and BC measurements were coincident

110   through the plume.

The collection optics were designed to maximize light capture despite any beam steering as the light transects the hot plume
gases. Although beam steering through hot flare plumes should be minimal, <1 mrad according to Conrad et al. (2020), any
light loss due to beam steering is necessarily interpreted as the presence of black carbon. To further minimize any potential

115   beam steering effects, a 0.75-m focal length plano-convex lens (Thorlabs, LA1978-C) was used to collect the light assuming
the beam was steered at the mid-point of the open path. The collected beam was focused to half its collimated diameter by a
set of plano-convex lenses (LA1134-C and LA1805-C, focal lengths of 60 mm and 30 mm, respectively) to ensure the beam
was smaller than the detector photodiode diameter. The two-wavelength beam was split into its constituent wavelengths by a
dichroic mirror (Thorlabs, DMLP1500R), passed through bandpass filters (FB1650-12 from Thorlabs, and 87-868 from

120   Edmund Optics), and directed onto transimpedance-amplified InGaAs detectors (Thorlabs, PDA20CS). Signals from all
detectors were recorded using a 1 MHz oscilloscope (National Instruments, PXIe-5172) and processed using software written
in LabVIEW.

The optical system was controlled by a National Instruments (NI) PXI base station which included the oscilloscope for reading

125   detector signals, a waveform generator used to sweep the laser injection current (NI, PXI-5406), and the laser driving systems.
The injection current of the H_2O detection laser was swept using a 200-Hz triangle waveform to allow the laser to scan back
and forth across the two absorption peaks of H_2O vapour centered at 7006.12 cm^{-1} (1427.32 nm) and 7007.03 cm^{-1}

(1427.14 nm) corresponding to combinational vibrational bands of $(2\nu_2+\nu_3)$ and $(\nu_1+\nu_3)$, respectively. Each 5-ms sweep period, consisting of a forward and backward scan of the H_2O peaks, was averaged to produce a single H_2O spectral signal for

130   analysis. The laser output wavelength throughout each sweep was determined using a gas reference cell (80-cm path length, containing 2.16% H_2O vapour by volume) in combination with a fiber-ring resonator (FRR) which had a free spectral range of 0.345 GHz ($0.0115\ cm^{-1}$). The H_2O absorption peaks observed in the reference cell served as absolute wavelength references while the optical resonance peaks of the FRR indicated the wavelength change throughout the laser sweep.

135   An estimate of the absorption-free intensity, necessary to quantify light attenuation during an experiment, was made before and after each experiment by placing a tube across the optical path and purging with N_2 gas for several minutes to remove the light absorbing species (*i.e.* ambient H_2O). Ambient H_2O concentrations could also be measured after the tube was removed and prior to lighting the flame. Signals collected during experiments were processed by subtracting the detector's measured dark current and then normalizing by the absorption-free intensity estimate to yield the measured transmissivity and hence

140   absorption.

3   Measurement Theory

3.1   Black Carbon Detection – Line-Of-Sight Attenuation (LOSA)

Soot/black carbon content in the flare plume was measured via optical attenuation of the 1654-nm laser, where the exact wavelength was tuned so that it was not detectably absorbed by H_2O, CO_2, CO, or methane. Following the definition of

145   Baumgardner et al. (2012), this approach of inferring soot volume fraction from light absorption yields estimates of "black carbon" (BC), which might alternatively be called "equivalent BC" (Andreae and Gelencsér, 2006; Petzold et al., 2013) or "light-absorbing carbon" (Bond and Bergstrom, 2006). In the specific context of gas flares, fresh particulate emissions are statistically pure elemental carbon (*e.g.* Conrad and Johnson, 2019; Popovicheva et al., 2019; Schwarz et al., 2015); thus, "elemental carbon", "soot", "(equivalent) black carbon", and "light-absorbing carbon" can be considered as synonymous in

150   the present work.

The optical transmissivity observed through a flare plume with the 1654-nm laser can be directly related to the soot/BC volume fraction through,

$$\tau = \frac{I}{I_0} = exp\left(-K_{e_\lambda}\int_s f_v(s)ds\right) \tag{1}$$

155   where K_{e_λ} [m^{-1}] is the BC extinction coefficient evaluated at some wavelength λ, f_v [-] is the local BC volume fraction which can be integrated over the optical path s [m], and the transmissivity τ [-] is calculated as a ratio of the measured (transmitted) intensity I over the incident intensity I_0 (Coderre et al., 2011; Migliorini et al., 2011). If the BC extinction coefficient K_{e_λ} is known at the operating wavelength, the transmissivity can be used to yield the integrated or path-averaged BC volume fraction.

From the review by Coderre et al. (2011), most rigorous soot optical property measurements in the literature have been
160 conducted in/near the visible region with most not exceeding 1064 nm in the infrared. Among the few studies investigating
soot optical properties between 1400-1700 nm, there is disagreement on K_{e_λ} values. However, this is not a limiting concern
in the present work, since any bias in assumed black carbon optical properties will affect absolute BC volume fractions but not
the strength of correlation with H_2O. Thus, BC optical properties at the measurement wavelength of 1654 nm were assumed
using complex refractive index values calculated from Chang & Charalampopoulos (1990) and a scattering-to-absorption ratio
165 extrapolated from Migliorini et al. (2011) to yield a reference extinction coefficient of 2.6×10^9 m^{-1}.

3.2 H₂O Absorption Spectra Isolation

The strongly light-absorbing black carbon will attenuate light at both laser wavelengths thereby corrupting the H_2O vapour
absorption spectra near 1428 nm. Given K_{e_λ} values at the two measurement wavelengths, a simple ratio of Eq. (1) at each
wavelength would be sufficient to isolate the H_2O absorption spectra from the attenuation caused by black carbon. Rather
170 than relying on the literature where there is some disagreement about K_{e_λ} values in the near infrared, an experiment was
conducted to estimate the ratio between BC extinction coefficients at 1654 nm and 1428 nm. This was accomplished by
producing a heavily-sooting ethylene flare and observing attenuation magnitudes at both wavelengths (while the 1428-nm laser
was tuned away from detectable H_2O absorption peaks). As detailed in the appendix, the experimentally determined BC
extinction coefficient ratio of $1.12 \pm 1.3 \times 10^{-4}$ fell within the range of values that could be calculated from the literature and
175 most closely resembled the results of Krishnan et al. (2001).

3.3 H₂O Detection – Tunable Diode Laser Absorption Spectroscopy (TDLAS)

The transmissivity of light through a light-absorbing gas medium is described by Beer-Lambert's law,

$$\tau(\nu) = \frac{I}{I_0} = \exp\left(-\int_s \frac{qp}{k_b T} \sigma(p, T, q, \nu) ds\right),$$ (2)

where $\tau(\nu)$ [-] is the optical transmissivity evaluated at some wavenumber ν [cm^{-1}], and the wavenumber is the inverse of the
180 incident radiation wavelength λ. $\tau(\nu)$ is related to local gas properties where q [-] is the volume fraction of the absorbing
species, p [Pa] is the pressure, and T [K] is the gas temperature. The equation also depends on Boltzmann's constant k_b
[$1.38064852 \times 10^{-19}$ (kg·cm^2)/(s^2·K)], and the absorption cross-section of the medium $\sigma(p, T, q, \nu)$ [cm^2/molecule] evaluated at
some wavenumber. Equation (2) is computed by integrating over the optical path, s [m]. Following the correction for black
carbon attenuation, and in the absence of other light absorbers at the chosen wavelength, $\sigma(p, T, q, \nu)$ for the isolated H_2O
185 absorption spectra were computed using the *HI*gh-resolution *TRAN*smission molecular absorption database (HITRAN), and
assuming a Lorentz profile to describe line broadening.

6

In the present application, the sample path is a line-of-sight (LOS) through a turbulent flare plume. This means that the integral

190 in Eq. (2) cannot be directly evaluated without knowledge of the temperature and volume fraction distribution along the measurement path. Instead, a technique called profile fitting, as implemented by Liu et al. (2007) in laminar flames, was employed here to deal with non-uniform gas properties along the LOS. The technique was selected since it was observed in preliminary simulations to have superior performance to other spectroscopic techniques developed for non-uniform sensing, at least in this application. Other techniques considered include integrated absorbance of two transitions (*e.g.* Farooq et al., 2008; Fotia et al., 2015; Liu et al.; Allen, 1998; Zhou et al., 2003) or multiple transitions in a linear regression solution (*e.g.*

195 Liu et al., 2013, 2005; Sanders et al., 2001; Zhang et al., 2016).

The profile fitting technique assumes that the unknown gas property distributions in Eq. (2) (in this case the H_2O volume fraction q, and temperature T) can be described by some general form. Here, we assume column ("tophat") distributions with identical column widths for both H_2O volume fraction and gas temperature as shown in Fig. 3. The column distributions are

200 a function of three independent unknowns to be solved (column width w, column temperature T_{col}, and column volume fraction q_{col}) and two constants (ambient temperature T_{amb}, and volume fraction q_{amb}) that can be directly measured. The assumed column distributions were substituted into Eq. (2) to compute theoretical absorption spectra which were compared with measured H_2O absorption signals. The parameters describing the column distributions (w, T_{col}, q_{col}) were then iteratively refined using a Nelder-Mead downhill simplex optimization scheme to best match the measured absorption spectra. The final

205 column distributions were used to compute path-averaged H_2O volume fractions for further analysis. Importantly, it is not critical to accurately reconstruct the spatial distribution of gas temperature and H_2O volume fraction along the path; the column distribution simply allows for meaningful path-average values to be calculated from an unknown distribution. Preliminary simulations also showed the column distribution approach to be more stable and accurate, at least in this application, than the Gaussian distribution approach proposed by Grauer et al. (2018).

210

A critical consideration for developing an optical system capable of measuring path-averaged H_2O volume fractions was the judicious selection of absorption transitions. After considering many potential transitions from the HITRAN database, a laser of 1428-nm nominal wavelength output was selected to measure two absorption peaks of H_2O vapour centered at 7006.12 cm^{-1} (1427.32 nm) and 7007.03 cm^{-1} (1427.14 nm), related to combinational vibrational bands of ($2\nu_2+\nu_3$) and

215 ($\nu_1+\nu_3$), respectively. These transitions were chosen because they had sufficient absorption strength to be measured in the lab, were isolated from other species transitions, and possessed the unique characteristic of having opposite, near-linear, scaling trends of peak absorption with increased temperature over the range of 300 K to 800 K. This last characteristic, related to their large difference in lower state energies, meant that temperature and concentration effects on the absorption peaks were effectively decoupled in the optimization scheme, increasing the overall accuracy of the method. Since expected flare plume

220 temperatures were <800 K (and most likely ≤600 K as suggested in thermocouple measurements by Poudenx et al., 2004),

these absorption transitions were ideally suited to this application. Poudenx et al.'s measurements were taken 1.4 m downstream of a 2.21-cm diameter flare with 2 m/s exit velocity. In this study, the measurements presented in Sect. 4 used flow velocities not exceeding 2 m/s and took LOS measurements at 2 m above the burner on buoyancy-driven turbulent flare plumes. Post-analysis of measurements presented in Sect. 4 confirmed that 95% of final measurements had path-averaged

225   temperatures <333 K and a maximum value of 384 K. Expected temperatures were thus also well below species reaction temperatures (*e.g.* adiabatic flame temperature of methane at 2224 K, thermal NO_x formation above ~1600 K) (Turns, 2000; U.S. EPA, 1999) meaning no major chemical reactions were occurring at the measurement height above the flare which would otherwise complicate measurements.

230   Prior to commencing experiments, the capabilities of the profile fitting technique were tested using the large eddy simulation (LES) data for methane flares in crossflow described by Conrad et al. (2020). Species and temperature data along chords through the simulated flare plume were extracted and used to compute simulated line-integrated signals (including added noise) that would be sensed by a detector. These test data included near-field locations with high peak temperatures and localized pockets of combustion products as well as far-field locations with lower peak temperatures and more dispersed combustion

235   products. For line-of-sight measurements where peak temperatures were below 800 K, the profile fitting technique accurately estimated the path-averaged H_2O volume fraction with a mean relative error of 0.3%; 95% of measurements were within ±3.2% relative error, and all were within ±6.3% relative error.
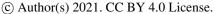
3.4 Experimental Acquisition and Processing

A typical pair of laser signals, following normalization by the absorption-free intensity estimates for each line, is shown in

240   Fig. 4 for an experiment running the Bakken flare gas mixture. The 1428-nm signal in Fig. 4a is the average of the lead and lag components of the 5-ms (200-Hz) triangle waveform sweep. The measurement from the 1654-nm laser shown in Fig. 4b was similarly averaged to allow for direct mapping of synchronous black carbon attenuation onto the 1428-nm signal. This allowed isolation of the H_2O spectra (shown in Fig. 5 plotted against wavenumber as determined using the FRR and reference cell signals). Overlaid in black on Fig. 5 is the fitted theoretical absorption spectrum produced by the column distributions as

245   determined by the Nelder-Mead algorithm; the residual plot above demonstrates the closeness of fit. The synchronous BC signal (Fig. 4b) was time-averaged over the sweep duration to obtain a single BC volume fraction for comparison with the H_2O estimate.

In the Nelder-Mead optimization scheme, a scalar sum-of-squared errors (SSE) value is produced representing the difference

250   between the measured and fitted path-averaged H_2O absorption spectra. A purposefully restrictive SSE threshold of $\leq 10^{-4}$ was used to filter the raw experimental data. Filtering on the basis of SSE is shown in the appendix to remove spectral data that is not well-fitted to a theoretical absorption peak during the profile fitting, potentially due to beam steering events. However, while this tight tolerance ensured robustness of the presented results, it is possible that this artificially reduces the variability

and skewness of the BC/H_2O ratio as elaborated in the appendix. For example, if cases of less than ideal spectral fitting are

255 correlated with instances in which complex turbulent structures in the plume allow BC and H_2O fluctuations to be uncorrelated, then the filtering could suppress part of the phenomena to be quantified. Future experiments with a faster time-resolution system and/or additional measured absorption lines could explore this further. For now, however, the presented correlation results likely represent a conservative lower bound on the spread and skewness of the BC/H_2O ratio.

4   Experimental Results and Discussion

260 Simultaneous path-averaged black carbon and H_2O volume fractions were recorded through plumes of flares over a range of flow rates and burner diameters. As summarized in Table 1, two main flare gas compositions were considered that were characteristic of flaring in the upstream oil and gas sector in the Bakken region of North Dakota (Brandt et al., 2016) and in Ecuador (Conrad and Johnson, 2017). These compositions were selected to consider a range of higher heating values which Conrad and Johnson (2017) suggested would produce differing sooting propensities. In addition, pure methane and pure

265 hydrogen tests were conducted to observe results in flares of low or zero black carbon content. Additional details of supporting experiments to measure the black carbon extinction coefficient ratio, constrain beam steering uncertainties, and assess the influence of measurement timescales are provided in the appendix.

Figure 6 shows example scatter plots of instantaneous path-averaged measurements of produced H_2O (measured H_2O volume

270 fraction minus measured ambient H_2O volume fraction) and BC volume fractions for two flare experiments. Although there is a general correlation between the species, as should be expected since the production of BC necessitates the production of H_2O vapour, the results show considerable scatter about the central trend. The variation is also not attributable to measurement noise which is more than an order of magnitude less than the apparent variation. As elaborated in the appendix, the anticipated error on the measured H_2O volume fraction was $\pm 3.0 \times 10^{-4}$ (relative error of $\pm 8.1\%$ at 95% confidence). For BC, the volume

275 fraction error is estimated to be $\pm 1.2 \times 10^{-10}$ (95% confidence). The low correlation coefficients of $R^2 = 0.50$ and 0.56 in Fig. 6 indicate that a substantial component of the variance is not explained by a simple linear model assuming perfect (time-invariant) correlation between species. Similar plots were seen for all test conditions with coefficients ranging from 0.40 to 0.67.

280 In the context of mass- or molar-balance approaches relying on a fixed ratio of species in space and/or time throughout the plume, histograms of BC/H_2O ratio data are plotted for each experiment in Fig. 7. Statistics for all cases, including hydrogen and methane control tests are summarized in Table 2. As apparent in Fig. 7, all of the experiments with realistic flare gas mixtures show similar distributions, with the BC/H_2O ratio varying about a single mode. Moreover, the distributions are all positively skewed, with a tail towards intermittent, higher values of the BC/H_2O ratio. There is no apparent trend with flare

285 gas flow rate or flare nozzle diameter, suggesting that the variation in BC/H_2O ratio is an inherent characteristic of the turbulent

Atmospheric
Measurement
Techniques
Discussions

buoyant plumes. There is, however, an apparent dependence on flare gas composition with the larger heating value Ecuador flare gas mixtures producing broader variation in BC/H_2O ratios (7.0–9.3 × 10^{-7} vs. 4.2–6.5 × 10^{-7}) than the Bakken flare measurements, as well as higher overall BC/H_2O ratios (20.0–24.8 × 10^{-7} vs. 11.6–15.0 × 10^{-7}). Data for each of these mixtures is aggregated in Table 2 and replotted in Fig. 8, where the skewness of the distributions becomes more apparent. On a relative

290 basis, the coefficient of variance (mean-normalized standard deviation) of the BC/H_2O ratios for the two mixtures are similar – 0.40 and 0.38, for Bakken and Ecuador mixtures, respectively. The skewness of the results aggregated by fuel type are also comparable (2.53 for Bakken and 2.30 for Ecuador). This again suggests that the uncorrelated variation in instantaneous species concentrations are most likely driven by turbulent dynamics within the heated, buoyant plume.

295 Prior to considering the possible implications of these results, it is first important to understand and bound the potential contributions of measurement uncertainty to the observed variability and skewness. Results of the hydrogen and methane tests were identically processed to glean the maximum amount of variability in an inferred BC/H_2O ratio that could be observable from measurement uncertainty alone. For the H_2 flame, there could be no black carbon produced, and any attenuation variation in the BC measurement laser would be solely attributable to experimental uncertainty. Similarly, any minor contribution from

300 BC in the methane control tests would only lead to a conservatively high estimate of uncertainty. Together, the hydrogen and methane control tests, with adiabatic flame temperatures of 2379 K and 2224 K, bound those of the experimental flare gas mixtures (2249 K and 2250 K) and thus should more than encompass the range of temperature-driven beam steering effects and thermally-driven fluid structures within the plume. The measured variability in the BC/H_2O ratio for the Bakken and Ecuador flare gas experiments exceeds the ratio variation of the control methane and hydrogen experiments by at least 3.7

305 times (median is a factor of 6.0).

In addition, a simple Monte Carlo (MC) simulation was performed to estimate BC/H_2O ratio variation and skewness attributable to measurement uncertainty, as further detailed in the appendix. The simulation took median BC and H_2O volume fraction results from Bakken and Ecuador datasets and computed ratios of the species volume fractions while including a

310 random, independently drawn contribution due to measurement uncertainty from distributions based on the control tests; further details are included in the appendix. Repeating this process 50,000 times produced a distribution of BC/H_2O ratios that represents a worst-case error bound since any correlation of uncertainty between the two species that might cancel when calculating their ratio was neglected. Statistics of the resulting distributions in BC/H_2O ratio after 50,000 iterations of the MC simulation are included in Table 2. Importantly, the experimentally measured variation in ratios for the realistic Bakken and

315 Ecuador flare gas mixtures is much larger than that which could be attributed to measurement uncertainty. The standard deviation was ~2.4–2.8 times larger and the skewness 4.6–7.2 times greater than what might be expected based on the Monte Carlo simulations (which represents a conservative upper bound on likely uncertainties as explained in Appendix A.5).

The measured BC/H_2O ratios of the Bakken and Ecuador flare gas mixtures, qualified by the control tests and Monte Carlo
320   simulations, point toward two important conclusions:

1)   Variability in instantaneous BC/H_2O ratios suggests the species are not always well-correlated in the turbulent plume; and

2)   Skewness of BC/H_2O ratio suggests the existence of short bursts of high black carbon production that are not well-correlated with H_2O.

The measured variability in path-averaged BC/H_2O ratios exceeds estimated measurement uncertainty and variability of
325   control tests and the variation is not symmetrical about the mean. The positive skewness of the BC/H_2O ratio suggests that
infrequent bursts of high BC/H_2O ratio heavily weight the mean value and populate the long tail of the distributions observed
in Fig. 8. This is interpreted physically as short bursts of high black carbon production that are not well-correlated with H_2O.
Short, infrequent, and localized bursts of high BC production have been previously observed by Conrad and Johnson (2017)
from sky-LOSA techniques measuring black carbon production from flares in Veracruz, Mexico and Orellana, Ecuador. Their
330   study demonstrated that overall BC emission rates are dominated by short bursts of high BC emission; in an extreme case,
10% of their instantaneous data corresponded to 56% of total emissions measured. What was not known in their study was
whether these high-sooting bursts were necessarily correlated with spikes in concentration of other combustion species such
that any ratio of species would be fixed. Experimental evidence from the current study suggests that this is unlikely. The
observed variability and positive skewness in the distribution of the measured BC/H_2O ratios suggests that that assumption of
335   a constant species ratios is not universally true which could limit the accuracy of field measurement techniques quantifying
flare performance based on short-duration measurements.

4.1 Implications for Field Measurements

The motivation of this study was to determine whether variations in species ratios in a turbulent plume could be detected, and
if so, to examine how these might affect field measurements that rely on the assumption of a fixed ratio as part of a molar- or
340   mass-balance to quantify pollutant emission rates or combustion efficiency, etc. Although a sufficiently long temporally- and
spatially-averaged species ratio measurement will approach some mean value for a given operating condition, the necessary
measurement time- or length-scales required for accurate estimates are not clear. Moreover, the effects of fluctuations in
relative species concentrations (*i.e.* species ratios) are exacerbated in measurement techniques that rely on a limited number
of measurements. For example, airborne measurements to obtain extractive samples during plume transects (*e.g.* Gvakharia
345   et al., 2017; Weyant et al., 2016) are often limited by cost and airtime, deriving data from 1 to 6 plume transects per flare.

As a thought experiment, if we assume that an aircraft or similar path-averaged technique randomly samples 1 to 6 draws from
the aggregated BC/H_2O histograms for the Bakken and Ecuador fuel mixtures (Fig. 8), this small sample size is unlikely to
obtain an accurate estimate of the mean BC/H_2O ratio. The skewed distribution means the calculated black carbon emission
350   rate from a small number of samples would more likely be biased low, potentially missing infrequent bursts of high BC
production. For any single measurement the most likely result would be the mode, which underestimates the mean ratio by

Atmospheric
Measurement
Techniques
Discussions

~13% for either fuel mixture. More importantly, however, the present results show how the broad variation in the ratios of instantaneous path-averaged species concentrations could introduce substantial additional uncertainty to measurements that assume these ratios are fixed.

355

A simple bootstrapping test was conducted to further consider the implications of undersampling. If we assume that some path-averaging measurement technique is sampling from either of the BC/H_2O ratio distributions in Fig. 8, these distributions can be randomly sampled (with replacement) to derive statistical criteria for the minimum required samples size required for a target level of accuracy. Histograms of the relative error of the calculated mean BC/H_2O ratio for a range of sample sizes

360 (each derived using 10,000 bootstrap trials) are plotted in Fig. 9. As should be expected, the potential error rapidly decreases as the sample size is increased. However, to be within a 10% error of the true mean BC/H_2O ratio, the results of Fig. 9 suggest ~100 measurements would be required. For a measurement limited to 5 samples, relative errors between –34% and +35% could be expected (95% confidence limits of the distribution), with the most likely outcome (modes of Fig. 9) being a 1–5% underestimate of the true value. With only two samples, this range of likely errors grows to –55% to +53%, with the modes

365 dropping to 2.5–7.5% below the mean.

It should be reiterated that these results are based on path-averaged measurements through vertical flare plumes. Weak instantaneous species correlations are arguably of even greater concern for techniques that employ point-sampling (*e.g.* drone-based measurements, Krause and Leirvik, 2018), which do not benefit from long path averages to smooth out relative species

370 variations. Indeed, time-averaged measurements of the compositional structure of flare plumes in a wind-tunnel show that spatial variation in relative species concentrations (specifically methane and CO_2) can be very large and, on their own (*i.e.* ignoring additional temporal effects), are sufficient to produce substantial variations in the locally calculated carbon conversion efficiency at different points within the plume (Poudenx, 2000). More generally, the influence of crosswind on the flare plume could be expected to exacerbate the presently observed temporal variations in relative species concentrations. While turbulent

375 plume motion could have beneficial mixing effects for some measurement approaches, this is not necessarily the case. High-frequency methane sampling measurements (Johnson et al., 2001) and flow visualization experiments (Johnson and Kostiuk, 2002) of flares in crossflow have also shown that methane can be emitted as intermittent bursts below the lee-side of a deflected flare flame, where these bursts are separated from the main CO_2-rich plume. These observations also suggest that the presently measured variation in BC/H_2O ratios is likely to extend to other species, notably unburned fuel and CO_2. Above all, the present

380 results suggest a need to carefully consider convergence criteria when designing and deploying measurement techniques that rely on an implicit assumption about temporally and spatially constant ratios of plumes species and a need for caution when interpreting measurements based on limited numbers of short-duration samples.

Atmospheric
Measurement
Techniques
Discussions

5 Conclusions

Experiments to measure the correlation between species in plumes of vertical, turbulent, buoyancy-driven flares have revealed
385 that instantaneous, path-averaged concentrations of black carbon (BC) and H_2O can vary independently and are not necessarily
well-correlated over short time intervals. Measurements using a novel tunable diode laser based optical system found
considerable scatter in the BC/H_2O ratio along a path through flare plumes that was well beyond that which could be attributed
to measurement uncertainty. Moreover, the distributions of BC/H_2O ratios suggest BC emissions are skewed by intermittent
bursts or fluctuations of high intensity, consistent with previous field observations. These results suggest that the common
390 assumption of fixed species ratios employed in many field measurement techniques is not universally valid and measurements
based on small numbers of samples, short time intervals, and/or limited spatial coverage of the plume would be subject to
potentially large added uncertainties. The positive skewness of the distribution of BC/H_2O volume fraction ratios also means
that techniques relying on limited numbers of samples are more likely to risk introducing a negative bias in inferred BC
emission rates. However, a bootstrap analysis of the present results also demonstrates how these issues can be readily avoided
395 with sufficient sample size and provides initial guidance for developing protocols for future field experiments using similar
path-averaged measurement approaches. Further study of the time- and length-scales that influence independent species
fluctuations are warranted, especially in the context of single-point sampling approaches (potentially including sampling via
remotely piloted aerial systems) which would not benefit from the optical path-averaging employed in the present experiments.

Appendix A   Quantification of Measurement Error

400 ### A.1   Spectral Profile Fitting Simulations

The performance of the optical measurement approach was first proven using large eddy simulation (LES) datasets of methane-
rich flares in crossflow described by Conrad et al. (2020). These simulations were of a 10-m tall, 102.3-mm diameter vertical
flare stack in crosswind and were designed to yield data representative of gas flaring operations in Alberta, Canada. The
simulated flare burned natural gas (90.53% methane, 3.73% ethane, 0.34% propane, 1.54% CO_2, and 3.86% N_2) at a stack exit
405 velocity of 4 m/s. The present study considered two of the crosswind cases, 1.11 m/s and 7.78 m/s, corresponding to the 10th
and 95th percentile windspeeds (simulations I and IV) in Conrad et al. (2020). Because the available simulation domain was
larger than the flare plumes produced at the Carleton University Flare Facility, the spatial domain was scaled down by a factor
of two (5 cm grid resolution was assigned to be 2.5 cm) noting that this would only increase the intensity of the variation along
the line-of-sight when testing the performance of the analysis algorithm.
410

Instantaneous line-of-sight (LOS) datasets from many different chords through the simulated flare plume were used to obtain
a wide variety of test conditions. These included samples in/near the flare where peak temperatures were high and combustion
species were localized, as well as far-field samples where gas mixing had drastically reduced peak temperatures and

combustion species were more dispersed along the LOS. The extracted LOS datasets from the flare simulations were 150 cm

415 long, the intended path length of the experimental setup, and were 60 nodes across. Theoretically measured H_2O spectra (*i.e.* the theoretical spectra reaching a detector after passing through the simulated plume domain) were generated by taking the product of the transmissivity through each node on the LOS, computed using the H_2O volume fraction and temperature and assuming a Lorentz lineshape. Because the flare simulations did not include detailed aerosol modelling, the spatial distributions of black carbon volume fraction were produced by scaling the combustion-derived CO_2 volume fraction by a

420 factor of 1/750,000 [−] to produce the optical attenuation values between 0 and 5% expected in laboratory experiments, similar to Conrad et al. (2020). It was not important that the absolute BC volume fractions be accurate, only that the distribution be representative of what might be found in a flare to facilitate testing of the analysis techniques. Black carbon attenuation along a LOS was calculated as the product of the BC attenuation at each node, knowing the local BC volume fraction, and assuming BC optical properties from the literature. BC extinction coefficients, K_{e_λ}, were assumed for each measurement wavelength

425 using complex index of refraction values calculated from Chang and Charalampopoulos (1990), and a BC scattering-to-absorption ratio estimated from Migliorini et al. (2011). The theoretical 1428-nm detector signal was a product of both BC attenuation and H_2O spectral absorption, whereas the 1654-nm signal was affected by BC attenuation only. Each of the calculated attenuation signals were intentionally corrupted with Gaussian-distributed noise with a standard deviation of 6×10^{-4} [−]. The level of added noise used was conservatively selected to be 50% larger than that measured during tests of the

430 experimental system. The ability of the analysis algorithm to correctly reproduce the path-averaged concentration from the noise-affected integrated signals was then quantitatively tested.

In the ~8,000 instantaneous simulation results, true path-averaged BC volume fraction results ranged from 0 to 15 ppb and were correctly estimated to within 0.02 ppb in all cases. The error in instantaneous path-averaged BC volume fraction estimates

435 was solely due to precision error caused by the corrupting noise. Path-averaged BC volume fraction estimates were then used to isolate the H_2O spectral absorption signal, as discussed in Sect. 3.2. The isolated H_2O signals were fitted with theoretical column distributions of H_2O volume fraction and temperature using a Nelder-Mead optimization scheme; the final calculated path-average H_2O fraction and temperature were then compared to the known path-averages from the LES simulations. Figure A1(a) shows a typical result of the column distribution fit, plotting the theoretical spectral absorption fitted to the simulated

440 measured signal. Figure A1(b) and (c) compare the fitted column distributions of H_2O volume fraction and temperature with the spatially-distributed LES data used to generate the measured signal. As indicated in the legend of Fig. A1(b), the path-averaged volume fraction in this example was estimated to within 1.2% of the true path-average. Similarly, the effective mean temperature was within 2 K of the true path-averaged value in Fig. A1(c).

445 By compiling all individual results, a trend of spectral fitting performance with peak gas temperature along the LOS for each measurement was observed. Figure A2 shows the relative error in path-averaged H_2O as a function of the peak gas temperature. The error in H_2O volume fraction appears to increase significantly with peak temperatures above roughly 800 K, which occurs

Atmospheric
Measurement
Techniques

Open Access

Discussions

EGU

in approximately 5% of the simulation results. This is likely due to the divergence of the transition linestrengths from near-linear beyond the range of 300 to 800 K. In practice, 95% of simulated measurements with peak LOS temperatures above 800 K produced a path-averaged temperature above 315 K, the median path-averaged temperature was 351 K. By comparison, 95% of the experimental path-averaged temperatures were below 334 and 333 K for Bakken and Ecuador tests, respectively. This gives some indication that peak temperatures in the experiment were not in excess of 800 K although these results are difficult to compare directly. However, as previously discussed, thermocouple measurements in plumes downstream of turbulent jet diffusion flames by Poudenx et al. (2004) suggest that temperatures do not typically exceed 600 K. Based on these results, the peak temperatures in the measured region of the present plumes are not expected exceed 800 K. Removing spectral fitting results from in-flame and with peak LOS temperatures in excess of 800 K, 95% of the ~7500 path-averaged H_2O volume fraction results were estimated to within ±3.2% with mean relative error of 0.32%; the maximum relative error was 6.3%.

An additional potential source of measurement error could arise due to temporal changes in the individual spectral signatures within the 5 ms (200 Hz) time-resolution of the H_2O measurement. Because the available LES data did not have sufficient time-resolution to investigate this issue, experimentally measured time-resolved BC attenuation data was instead used to produce synthetic time-varying H_2O volume fraction data to estimate effects of temporal averaging of spectral signals. As discussed further in Seymour (2019), the results suggest a mean relative error of 0.28% for path-averaged H_2O volume fractions where 95% of measurements were within ±5.1%. Assuming temporal and spatial error estimated for path-averaged H_2O volume fraction are independent, the values were combined in quadrature that resulted in a mean error of 0.63% with 95% of measurements falling within ±8.1%.

A.2   Beam Steering Effects on Measurements

Although the optical system was meticulously aligned prior to each experiment and simulations by Conrad et al. (2020) suggest beam steering through turbulent flare plumes should not exceed 1 mrad, beam steering effects in the present experiments cannot be completely discounted because the location and orientation of the highest temperature gradients is invariably unknown. Because beam steering would result in a loss or gain of light into the detectors, it would necessarily be interpreted as fluctuations in plume transmissivity and therefore BC presence. To experimentally quantify light loss due to beam steering, tests were completed on a flare burning pure hydrogen at 150 SLPM on the 25.4-mm diameter burner. The 1654-nm laser was then used to acquire transmissivity measurements in the absence of BC. A histogram of laser signal attenuation, and apparent BC presence, for a 2-minute period is shown in Fig. A3. In this hydrogen flare test, where no BC is produced, the system observes an apparent path-averaged mean BC volume fraction of -2.1×10^{-12} (*i.e.* centered about zero) with a standard deviation of 3.2×10^{-10}. By comparison, the Bakken and Ecuador tests showed variations of 1.03×10^{-9} and 1.66×10^{-9} centered about mean values of 2.39×10^{-9} and 3.69×10^{-9}, respectively. Therefore, 95% of the measurements presented

Atmospheric
Measurement
Techniques
Discussions

480   in Sect. 4 for Bakken and Ecuador flare gas have a BC signal-to-noise ratio (SNR) of at least 4 times the H_2 standard deviation; the median SNR is ~12.

Although the two laser beams were collinear through the heated plume, they were ultimately focused onto two separate targets meaning that it was still possible to have some relative differences in the signals due to beam steering. To bound the potential

485   impact of this effect, attenuation differences between the two laser signals were recorded through plumes of a hydrogen flare, whose adiabatic flame temperature (2379 K) exceeded that of all other flare tests, providing an upper limit to the magnitudes of temperature gradient-driven beam steering. The 1428-nm laser was tuned to a minimum H_2O absorption wavelength of 7009.25 cm^{-1} (1426.69 nm), where it was estimated that the H_2O fluctuations would not contribute absorption magnitudes higher than 0.03%, and attenuation data was recorded for both laser lines. The differences in attenuation magnitude between

490   synchronous points from each laser were centred about zero (mean of 0.007%) with a standard deviation of 0.16% suggesting that 95% of measurements had attenuation differences of less than 0.31%. For reference, the main peak of interest to be measured varied between 2 and 6% absorption, *i.e.*, between 6.5 and 20 times higher signal amplitude in all cases. Although this will cause some distortion in the H_2O absorption spectra, the profile fitting algorithm with goodness-of-fit filter was able to identify cases where beam steering produced poor fitting results as explained in Section A.4 below.

495 **A.3**   **Black Carbon Optical Property Ratio Measurements**

As discussed in Section 3.2, a ratio of black carbon (BC) extinction coefficient (K_{e_λ}) values at the two laser wavelengths was required to isolate the H_2O absorption spectra in the presence of broadband BC attenuation. Since there was disagreement in the literature about BC optical properties in the near infrared, the ratio of optical properties used in the present analysis was measured experimentally. Using a heavily-sooting ethylene flare at 50 SLPM on the 76.2-mm diameter burner attenuation

500   measurements were recorded at the two laser wavelengths, 1654 nm and 1428 nm. The 1428-nm laser was tuned off of detectable H_2O absorption peaks to solely measure BC attenuation through the plume. The extinction coefficient ratio (ECR) between the measurement wavelengths was calculated for conditions with at least 5% attenuation along the path (giving a SNR of >30) using Eq (1) and the experimental data are shown in Fig. A4 overlaid with values calculated from the literature. The mean BC extinction coefficient ratio ($K_{e_{1428}}/K_{e_{1654}}$) was 1.12 with a standard error of the mean of 1.3×10^{-4}. The resulting

505   ECR estimate is bounded by values calculated from extinction experiments in the literature (Table A1) and most closely resembles the result calculated using data from Krishnan et al. (2001). This necessary result permits the isolation of spectral H_2O absorption in subsequent measurements.

A.4   **BC/H_2O Ratio Data Filtering**

As noted in Sect. 3.4, experimental data were filtered based on the closeness of fit between the measured H_2O spectra and

510   theoretical spectra produced by the Nelder-Mead fitting algorithm, as characterized by the scalar sum-of-squared errors (SSE).

The purpose of this filtering was to reduce uncertainty by removing cases where the spatial or temporal changes in H_2O volume fraction and/or temperature rendered spectra difficult to describe with a column distribution. As argued in the main text, a conservative SSE cut-off of 10^{-4} [-] was applied, following an investigation of the effects of the chosen SSE cut-off on distributions of the measured BC/H_2O ratio.

515

The maximum SSE cut-off of 10^{-4} [-] was selected, corresponding to the largest SSE value measured during controlled H_2O vapour measurements in an optical flow-through cell (Seymour, 2019). This implied an expected upper bound error for fitting of real-world spectra with theory. Subsequent analysis revealed that this choice is conservative, such that raising this filter threshold only increased the range of measured BC/H_2O ratios and heightened the skewness of the distribution. This was
520 demonstrated by reprocessing the experimental datasets with a range of SSE filter values and recomputing the BC/H_2O ratio variability and skewness. Figure A5 shows the filtering effect on standard deviation (a-b) and skewness (c-d) for the two fuel compositions. Less restrictive SSE filter settings only increase the variability and skewness of the BC/H_2O ratio data.

A.5 Upper Bound Potential Influence of Uncertainty on BC/H_2O Ratio Distributions

To bound the potential influence of measurement uncertainty on the measured variations in the BC/H_2O ratio, a simple Monte
525 Carlo simulation was conducted. As described in Sect. A.1, the H_2O measurement had a mean relative error of 0.63% with a standard deviation of 4.1%; for BC, the mean relative error was 0.007% and the standard deviation was 0.16%. In Sect. A.2, hydrogen flare experiments suggest beam steering produces an apparent path-averaged mean BC volume fraction of no more than -2.1×10^{-12} with a standard deviation of 3.18×10^{-10}. Random draws of these experimentally-determined measurement uncertainties were independently applied to the median BC and H_2O volume fraction results from the Bakken and Ecuador
530 datasets. The distribution of BC/H_2O ratios about the median BC/H_2O ratio (*i.e.* the distribution of results attributable to measurement uncertainty alone) were then plotted and overlaid on the experimental results for the Bakken and Ecuador fuel mixtures as shown in Fig. A6. It should be noted that by assuming measurement uncertainties on the BC and H_2O signals are completely uncorrelated, this approach gives a conservative upper-bound on the potential effect of uncertainty on the BC/H_2O ratio measurement.

535

As summarized in Table 2 of the main text, the Monte Carlo results, suggest that the maximum variation in the measured BC/H_2O ratio that could be attributable to uncertainty had a standard deviation of 2.3×10^{-7} and 3.1×10^{-7} and skewness of 0.35 and 0.50 for Bakken and Ecuador mixture experiments, respectively. The Bakken and Ecuador experiments exceeded the Monte Carlo standard deviations by factors of 2.4 and 2.8, and skewness by factors of 7.2 and 4.6, respectively. As overlaid
540 in Fig. A6, the experimentally observed variation in the BC/H_2O ratio is notably larger, and the skewness notably stronger, than the upper bound estimate of what might be attributable to measurement uncertainty alone.

550

Author contributions:

MRJ and SPS contributed to the conception and design. SPS performed the acquisition of data. SPS and MRJ contributed to
analysis and interpretation of data, drafting and revising of the article, and approved the submitted version for publication.

555 *Competing interests:*

The authors have no known competing financial interests or personal relationships that could have appeared to influence the
work reported in this paper.

565

References

Andreae, M. O. and Gelencsér, A.: Black carbon or brown carbon? The nature of light-absorbing carbonaceous aerosols,
Atmos. Chem. Phys., 6(10), 3131–3148, doi:10.5194/acp-6-3131-2006, 2006.

Baumgardner, D., Popovicheva, O. B., Allan, J., Bernardoni, V., Cao, J., Cavalli, F., Cozic, J., Diapouli, E., Eleftheriadis, K.,
570 Genberg, P. J., Gonzalez, C., Gysel, M., John, A., Kirchstetter, T. W., Kuhlbusch, T. A. J., Laborde, M., Lack, D., Müller, T.,
Niessner, R., Petzold, A., Piazzalunga, A., Putaud, J. P., Schwarz, J., Sheridan, P., Subramanian, R., Swietlicki, E., Valli, G.,
Vecchi, R. and Viana, M.: Soot reference materials for instrument calibration and intercomparisons: a workshop summary
with recommendations, Atmos. Meas. Tech., 5(8), 1869–1887, doi:10.5194/amt-5-1869-2012, 2012.

Blackwood, T. R.: An evaluation of flare combustion efficiency using open-path Fourier transform infrared technology., J. Air
575 Waste Manage. Assoc., 50(10), 1714–22, 2000.

Blokh, A. G.: Heat Transfer In Steam Boiler Furnaces, 1st ed., CRC Press., 1988.

Bond, T. C. and Bergstrom, R. W.: Light Absorption by Carbonaceous Particles: An Investigative Review, Aerosol Sci. Technol., 40(1), 27–67, doi:10.1080/02786820500421521, 2006.

Bond, T. C., Doherty, S. J., Fahey, D. W., Forster, P. M., Berntsen, T. K., DeAngelo, B. J., Flanner, M. G., Ghan, S., Kärcher,
580 B., Koch, D., Kinne, S., Kondo, Y., Quinn, P. K., Sarofim, M. C., Schultz, M. G., Schulz, M., Venkataraman, C., Zhang, H., Zhang, S., Bellouin, N., Guttikunda, S. K., Hopke, P. K., Jacobson, M. Z., Kaiser, J. W., Klimont, Z., Lohmann, U., Schwarz, J. P., Shindell, D. T., Storelvmo, T., Warren, S. G. and Zender, C. S.: Bounding the role of black carbon in the climate system: A scientific assessment, J. Geophys. Res. Atmos., 118(11), 5380–5552, doi:10.1002/jgrd.50171, 2013.

Brandt, A. R., Yeskoo, T., McNally, M. S., Vafi, K., Yeh, S., Cai, H. and Wang, M. Q.: Energy intensity and greenhouse gas
585 emissions from tight oil production in the Bakken formation, Energy & Fuels, 30(11), 9613–9621, doi:10.1021/acs.energyfuels.6b01907, 2016.

Cape, J. N., Coyle, M. and Dumitrean, P.: The atmospheric lifetime of black carbon, Atmos. Environ., 59, 256–263, doi:10.1016/j.atmosenv.2012.05.030, 2012.

Chang, H. and Charalampopoulos, T. T.: Determination of the Wavelength Dependence of Refractive Indices of Flame Soot,
590 Proc. R. Soc. A Math. Phys. Eng. Sci., 430(1880), 577–591, doi:10.1098/rspa.1990.0107, 1990.

Coderre, A. R., Thomson, K. A., Snelling, D. R. and Johnson, M. R.: Spectrally-Resolved Light Absorption Properties of Cooled Soot from a Methane Flame, Appl. Phys. B, 104(1), 175–188, doi:10.1007/s00340-011-4448-9, 2011.

Conrad, B. M. and Johnson, M. R.: Field measurements of black carbon yields from gas flaring, Environ. Sci. Technol., 51(3), 1893–1900, doi:10.1021/acs.est.6b03690, 2017.

595 Conrad, B. M. and Johnson, M. R.: Mass absorption cross-section of flare-generated black carbon: Variability, predictive model, and implications, Carbon N. Y., 149, 760–771, doi:10.1016/j.carbon.2019.04.086, 2019.

Conrad, B. M., Thornock, J. N. and Johnson, M. R.: Beam steering effects on remote optical measurements of pollutant emissions in heated plumes and flares, J. Quant. Spectrosc. Radiat. Transf., 254, doi:10.1016/j.jqsrt.2020.107191, 2020.

Farooq, A., Jeffries, J. B. and Hanson, R. K.: In situ combustion measurements of H_2O and temperature near 2.5 μm using
600 tunable diode laser absorption, Meas. Sci. Technol., 19(7), 075604, doi:10.1088/0957-0233/19/7/075604, 2008.

Flanner, M. G.: Arctic climate sensitivity to local black carbon, J. Geophys. Res. Atmos., 118(4), 1840–1851, doi:10.1002/jgrd.50176, 2013.

Fotia, M. L., Sell, B. C., Hoke, J., Wakefield, S. and Schauer, F.: 1 kHz Mid-IR Absorption Spectroscopy for CO and CO 2 Concentration and Temperature Measurement, Combust. Sci. Technol., 187(12), 1922–1936,
605 doi:10.1080/00102202.2015.1069281, 2015.

Gasser, T., Peters, G. P., Fuglestvedt, J. S., Collins, W. J., Shindell, D. T. and Ciais, P.: Accounting for the climate-carbon feedback in emission metrics, Earth Syst. Dyn., 8(2), 235–253, doi:10.5194/esd-8-235-2017, 2017.

Grauer, S. J., Conrad, B. M., Miguel, R. B. and Daun, K. J.: Gaussian Model for Emission Rate Measurement of a Heated Plume using Hyperspectral Data, J. Quant. Spectrosc. Radiat. Transf., 206, 125–134, doi:10.1016/j.jqsrt.2017.11.005, 2018.

610   Gvakharia, A., Kort, E. A., Brandt, A. R., Peischl, J., Ryerson, T. B., Schwarz, J. P., Smith, M. L. and Sweeney, C.: Methane, black carbon, and ethane emissions from natural gas flares in the Bakken Shale, North Dakota, Environ. Sci. Technol., 51(9), 5317–5325, doi:10.1021/acs.est.6b05183, 2017.

Herndon, S. C., Nelson, D. D., Wood, E. C., Knighton, W. B., Kolb, C. E., Kodesh, Z., Torres, V. M. and Allen, D. T.: Application of the Carbon Balance Method to Flare Emissions Characteristics, Ind. Eng. Chem. Res., 51(39), 12577–12585,
615   doi:10.1021/ie202676b, 2012.

Jacobson, M. Z.: Short-term effects of controlling fossil-fuel soot, biofuel soot and gases, and methane on climate, Arctic ice, and air pollution health, J. Geophys. Res., 115(D14209), 1–24, doi:10.1029/2009JD013795, 2010.

Johnson, M. R. and Kostiuk, L. W.: Visualization of the fuel stripping mechanism for wake-stabilized diffusion flames in a crossflow, in IUTAM Symposium on Turbulent Mixing and Combustion, vol. 70, edited by A. Pollard and S. Candel, pp. 295–
620   303, Springer Netherlands, Dordrecht., 2002.

Johnson, M. R., Wilson, D. J. and Kostiuk, L. W.: A fuel stripping mechanism for wake-stabilized jet diffusion flames in crossflow, Combust. Sci. Technol., 169(1), 155–174, doi:10.1080/00102200108907844, 2001.

Klimont, Z., Kupiainen, K., Heyes, C., Purohit, P., Cofala, J., Rafaj, P., Borken-Kleefeld, J. and Schöpp, W.: Global anthropogenic emissions of particulate matter including black carbon, Atmos. Chem. Phys., 17(14), 8681–8723,
625   doi:10.5194/acp-17-8681-2017, 2017.

Köylü, Ü. Ö. and Faeth, G. M.: Optical properties of overfire soot in buoyant turbulent diffusion flames at long residence times, J. Heat Transfer, 116(1), 152–159, doi:10.1115/1.2910849, 1994.

Krause, D. F. and Leirvik, F.: Field Measurement of BC Emissions from Rolvsnes Well Test Flare., 2018.

Krishnan, S. S., Lin, K.-C. and Faeth, G. M.: Extinction and Scattering Properties of Soot Emitted From Buoyant Turbulent
630   Diffusion Flames, J. Heat Transfer, 123(2), 331, doi:10.1115/1.1350823, 2001.

Liu, C., Xu, L. and Cao, Z.: Measurement of nonuniform temperature and concentration distributions by combining line-of-sight tunable diode laser absorption spectroscopy with regularization methods, Appl. Opt., 52(20), 4827, doi:10.1364/AO.52.004827, 2013.

Liu, J. T. C., Rieker, G. B., Jeffries, J. B., Gruber, M. R., Carter, C. D., Mathur, T. and Hanson, R. K.: Near-infrared diode
635   laser absorption diagnostic for temperature and water vapor in a scramjet combustor, Appl. Opt., 44(31), 6701, doi:10.1364/AO.44.006701, 2005.

Liu, X., Jeffries, J. B., Hanson, R. K., Hinckley, K. M. and Woodmansee, M. A.: Development of a tunable diode laser sensor for measurements of gas turbine exhaust temperature, Appl. Phys. B Lasers Opt., 82(3), 469–478, doi:10.1007/s00340-005-2078-9, 2006.

640   Liu, X., Jeffries, J. B. and Hanson, R. K.: Measurement of Non-Uniform Temperature Distributions Using Line-of-Sight Absorption Spectroscopy, AIAA J., 45(2), 411–419, doi:10.2514/1.26708, 2007.

Mark, G. A.: Diode laser absorption sensors for gas-dynamic and combustion flows, Meas. Sci. Technol., 9(4), 545 [online] Available from: http://stacks.iop.org/0957-0233/9/i=4/a=001, 1998.

Atmospheric
Measurement
Techniques
Discussions

Migliorini, F., Thomson, K. A. and Smallwood, G. J.: Investigation of optical properties of aging soot, Appl. Phys. B Lasers
645   Opt., 104(2), 273–283, doi:10.1007/s00340-011-4396-4, 2011.

Petzold, A., Ogren, J. A., Fiebig, M., Laj, P., Li, S.-M., Baltensperger, U., Holzer-Popp, T., Kinne, S., Pappalardo, G.,
Sugimoto, N., Wehrli, C., Wiedensohler, A. and Zhang, X.-Y.: Recommendations for reporting "black carbon" measurements,
Atmos. Chem. Phys., 13(16), 8365–8379, doi:10.5194/acp-13-8365-2013, 2013.

Pohl, J. H., Tichenor, B. A., Lee, J. and Payne, R.: Combustion Efficiency of Flares, Combust. Sci. Technol., 50(4–6), 217–
650   231, doi:10.1080/00102208608923934, 1986.

Popovicheva, O. B., Timofeev, M. A., Persiantseva, N., Jefferson, M. A., Johnson, M., Rogak, S. N. and Baldelli, A.:
Microstructure and Chemical Composition of Particles from Small-scale Gas Flaring, Aerosol Air Qual. Res., 19(10), 2205–
2221, doi:10.4209/aaqr.2019.04.0177, 2019.

Poudenx, P.: Plume sampling of a flare in crosswind: structure and combustion efficiency, M.Sc. Thesis, University of Alberta,
655   Edmonton, AB, Canada, Edmonton., 2000.

Poudenx, P., Howell, L. W., Wilson, D. J. and Kostiuk, L. W.: Downstream Similarity of Thermal Structure in Plumes From
Jet Diffusion Flames in a Crossflow, Combust. Sci. Technol., 176(3), 409–435, doi:10.1080/00102200490270139, 2004.

Ramanathan, V. and Carmichael, G.: Global and regional climate changes due to black carbon, Nat. Geosci., 1(4), 221–227,
doi:10.1038/ngeo156, 2008.

660   Sand, M., Berntsen, T. K., Von Salzen, K., Flanner, M. G., Langner, J. and Victor, D. G.: Response of Arctic temperature to
changes in emissions of short-lived climate forcers, Nat. Clim. Chang., 6(3), 286–289, doi:10.1038/nclimate2880, 2016.

Sanders, S. T., Wang, J., Jeffries, J. B. and Hanson, R. K.: Diode-laser absorption sensor for line-of-sight gas temperature
distributions, Appl. Opt., 40(24), 2001.

Schwarz, J. P., Holloway, J. S., Katich, J. M., McKeen, S., Kort, E. A., Smith, M. L., Ryerson, T. B., Sweeney, C. and Peischl,
665   J.: Black carbon emissions from the Bakken oil and gas development region, Environ. Sci. Technol. Lett., 2(10), 281–285,
doi:10.1021/acs.estlett.5b00225, 2015.

Seymour, S. P.: Spectroscopic Measurements of Path-Averaged Species Correlations in Turbulent Flare Plumes, Carleton
University., 2019.

Strosher, M. T.: Characterization of emissions from diffusion flare systems, J. Air Waste Manage. Assoc., 50(10), 1723–33,
670   2000.

Turns, S. R.: An Introduction to Combustion: Concepts and Applications, 2nd ed., McGraw-Hill, USA., 2000.

U.S. EPA: Nitrogen Oxides (NOx), Why and How They Are Controlled., 1999.

U.S. EPA: Report to Congress on Black Carbon, United States Environmental Protection Agency (U.S. EPA), Research
Triangle Park, NC., 2012.

675   Weyant, C. L., Shepson, P. B., Subramanian, R., Cambaliza, M. O. L. L., Heimburger, A., Mccabe, D., Baum, E., Stirm, B.
H. and Bond, T. C.: Black carbon emissions from associated natural gas flaring, Environ. Sci. Technol., 50(4), 2075–2081,
doi:10.1021/acs.est.5b04712, 2016.

Winiger, P., Barrett, T. E., Sheesley, R. J., Huang, L., Sharma, S., Barrie, L. A., Yttri, K. E., Evangeliou, N., Eckhardt, S., Stohl, A., Klimont, Z., Heyes, C., Semiletov, I. P., Dudarev, O. V., Charkin, A., Shakhova, N., Holmstrand, H., Andersson, A. and Gustafsson, Ö.: Source apportionment of circum-Arctic atmospheric black carbon from isotopes and modeling, Sci. Adv., 5(2), eaau8052, doi:10.1126/sciadv.aau8052, 2019.

680

World Bank: Global Gas Flaring Jumps to Levels Last Seen in 2009, [online] Available from: https://www.worldbank.org/en/news/press-release/2020/07/21/global-gas-flaring-jumps-to-levels-last-seen-in-2009 (Accessed 4 February 2021), 2020.

685 Wormhoudt, J., Herndon, S. C., Franklin, J., Wood, E. C., Knighton, B., Evans, S., Laush, C., Sloss, M. and Spellicy, R.: Comparison of remote sensing and extractive sampling measurements of flare combustion efficiency, Ind. Eng. Chem. Res., 51(39), 12621–12629, doi:10.1021/ie202783m, 2012.

Zhang, G., Liu, J., Xu, Z., He, Y. and Kan, R.: Characterization of temperature non-uniformity over a premixed CH_4-air flame based on line-of-sight TDLAS, Appl. Phys. B Lasers Opt., 122(1), 1–9, doi:10.1007/s00340-015-6289-4, 2016.

690 Zhao, Y., Nielsen, C. P., Lei, Y., McElroy, M. B. and Hao, J.: Quantifying the uncertainties of a bottom-up emission inventory of anthropogenic atmospheric pollutants in China, Atmos. Chem. Phys., 11(5), 2295–2308, doi:10.5194/acp-11-2295-2011, 2011.

Zhou, X., Liu, X., Jeffries, J. B. and Hanson, R. K.: Development of a sensor for temperature and water concentration in combustion gases using a single tunable diode laser, Meas. Sci. Technol., 14(8), 1459–1468, doi:10.1088/0957-0233/14/8/335,

695 2003.

Zhu, J., Choi, M. Y., Mulholland, G. W., Manzello, S. L., Gritzo, L. a. and Suo-Anttila, J.: Measurement of visible and near-IR optical properties of soot produced from laminar flames, Proc. Combust. Inst., 29(2), 2367–2374, doi:10.1016/S1540-7489(02)80288-7, 2002.
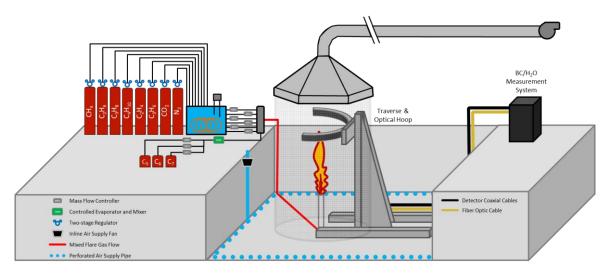
Figure 1: Schematic of the Carleton University Flare Facility (CUFF) showing the mounting "hoop" for the optics that were positioned above the flare by a 3-axis traverse system.
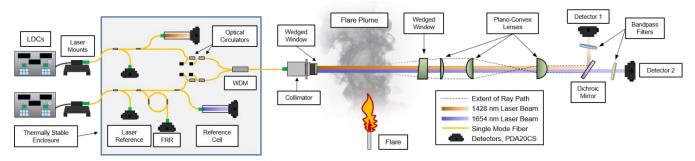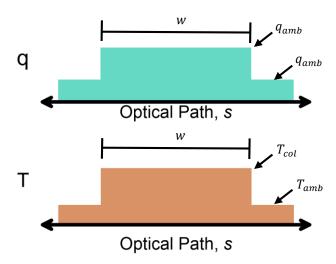
700

Figure 2: Schematic of the optical measurement system for measuring synchronous path-averaged BC and H_2O volume fractions along a path through the flare plume. Components within the shaded box were temperature stabilized within a thermo-electric heater/cooler. Dashed lines representing ray path extent shown how optical arrangement minimizes any effects of beam steering through the plume.

705

Atmospheric
Measurement
Techniques
Discussions

710 **Figure 3: Column distribution of temperature and H_2O volume fraction used to generate theoretical spectra for comparison with measured data.**

Table 1: Experimental fuel compositions in volume fraction [%] with their molecular weight (MW), volumetric higher heating value (HHV$_v$), and molar carbon-hydrogen ratio (CHR). Prefixes "n" and "i" distinguish between straight- and branched-chain isomers,
715 **where appropriate, of the C1-C7 alkanes.**

Fuel Name	C1	C2	C3	nC4	iC5	nC6	nC7	H$_2$	N$_2$	CO$_2$	CHR [–]	MW [g/mol]	HHV$_v$ [MJ/m³]
Bakken (BK)[a]	49.12	20.97	15.04	6.72	2.15	0.87	0.78	0	3.66	0.70	0.331	29.13	64.33
Ecuador (EC)[b]	40.82	8.16	16.93	14.75	6.81	2.06	1.38	0	3.37	5.71	0.364	36.57	75.17

[a] Mean gas compositions from roughly 700 wells in Bakken region (Brandt et al., 2016)
[b] Selected gas composition from Ecuador's Orellana province (Conrad and Johnson, 2017)

Figure 4: Sample 5 ms duration measurement of (a) 1428 nm (H₂O+BC) and (b) 1654 nm (BC) laser signals through a Bakken flare plume. Time-resolved signals can be mapped to isolate spectral H₂O absorption peaks from black carbon.
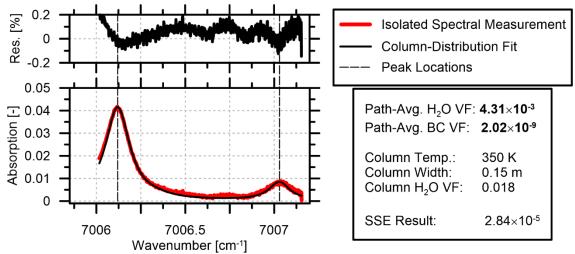

Figure 5: H₂O absorption peaks in isolated, spectrally-resolved form compared to the column distribution result from the NM optimization search.
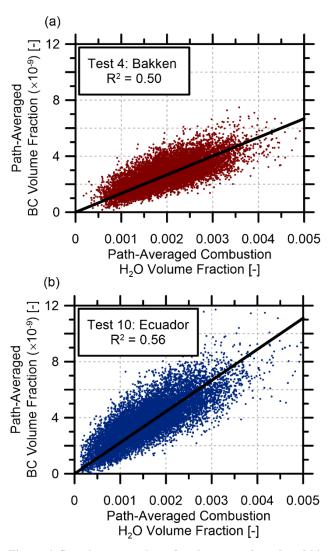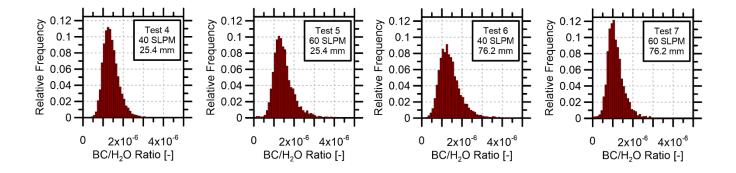
Atmospheric
Measurement
Techniques
Discussions

Figure 6: Sample scatter plots of path-averaged produced black carbon (BC) and H₂O volume fractions for (a) Bakken fuel test 4 (40 SLPM, 25.4 mm burner), (b) Ecuador fuel test 10 (40 SLPM, 76.2-mm burner).

725

730

Figure 7: Black Carbon (BC)/H₂O volume fraction ratios for tests with the Bakken flare gas mixture (top row), and Ecuador flare gas mixture (bottom row).

Table 2: Summary of Flare Test Black Carbon/H₂O Ratio Results and Relevant Statistics

Test ID.	Fuel Type	Test Condition	Points	Mean BC/H_2O Ratio [-] ($\times 10^{-7}$)	BC/H_2O Std. Dev. [-] ($\times 10^{-7}$)	Coeff. of Variation [-]	Skewness
Control-1	Hydrogen	150 SLPM, 25.4 mm	9613	0.11	1.13	*10.27*[b]	*1.47*[b]
Control-2	Methane	40 SLPM, 25.4 mm	2349	1.11	0.85	*0.77*[b]	*1.23*[b]
Control-3		60 SLPM, 25.4 mm	7426	-0.14[a]	0.77	*-5.50*[b]	*1.06*[b]
Exp-4	Bakken	40 SLPM, 25.4 mm	13015	14.06	4.17	0.30	1.53
Exp-5		60 SLPM, 25.4 mm	4019	14.95	6.46	0.43	3.13
Exp-6		40 SLPM, 76.2 mm	13656	14.34	6.31	0.44	2.36
Exp-7		60 SLPM, 76.2 mm	3669	11.61	4.92	0.42	3.36
Exp-8	Ecuador	40 SLPM, 25.4 mm	4854	19.97	6.95	0.35	1.18
Exp-9		60 SLPM, 25.4 mm	1526	21.26	9.34	0.44	1.89
Exp-10		40 SLPM, 76.2 mm	14007	24.80	9.02	0.36	2.35
Exp-11		60 SLPM, 76.2 mm	4747	22.72	8.93	0.39	3.10
CH₄-Agg	**Methane - Aggregated**	**Various**	**9,775**	**0.16**	**0.95**	**5.94**	**0.96**
BK-Agg	**Bakken - Aggregated**		**34,359**	**14.01**	**5.54**	**0.40**	**2.53**
EC-Agg	**Ecuador - Aggregated**		**25,134**	**23.26**	**8.87**	**0.38**	**2.30**
BK-MC	**Bakken – Monte Carlo**	**Various**	**50,000**	**13.27**	**2.28**	**0.17**	**0.35**
EC-MC	**Ecuador – Monte Carlo**	**Various**	**50,000**	**22.46**	**3.13**	**0.14**	**0.50**

[a] This non-physical value of the BC/H_2O ratio is a result of system noise and uncertainty on a BC signal near zero for the pure methane flame suggesting BC may not be sufficiently detectable for the methane experiment.

[b] Coefficients of variation and skewness for the control tests are included for completion but are not meaningful since the mean BC/H_2O ratios are near zero for these tests and the absolute variations (as measured by the standard deviation) are much smaller than those of the experimental cases.
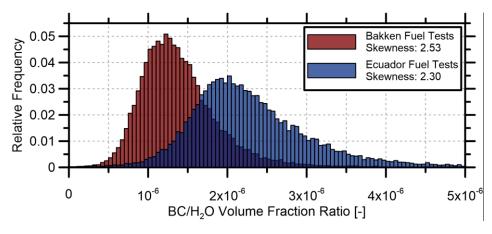
735

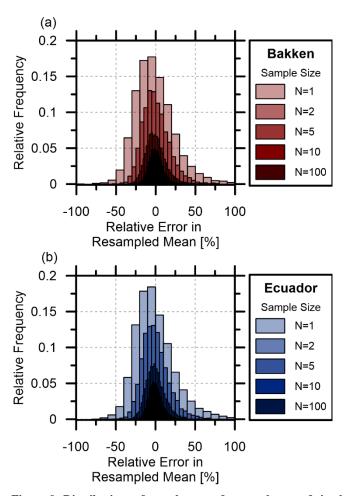**Figure 8: Combined BC/H₂O ratio distributions for the two fuel types presented.**

740

Figure 9: Distributions of sample mean for sample sets of size *N* from BC/H$_2$O ratio results of (a) Bakken and (b) Ecuador flare tests.
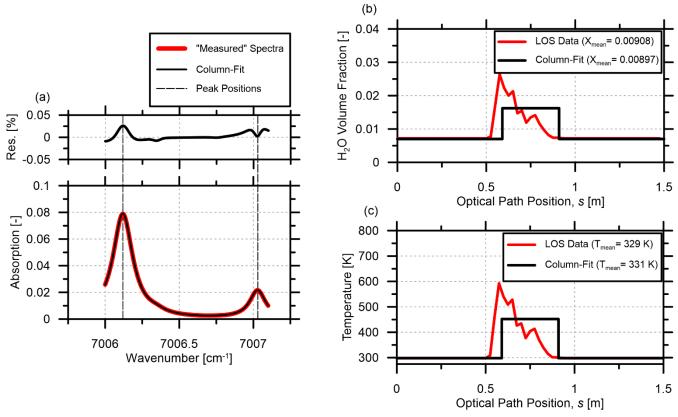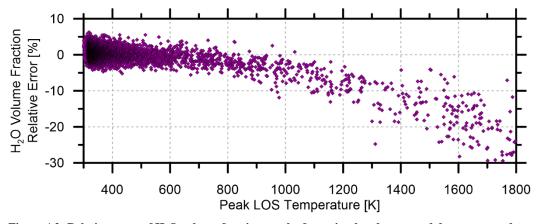
745

Figure A1: Sample profile fitting result where (a) compares the column distribution spectra to the simulated measured spectra, and (b) and (c) compare the column distribution profiles with LOS simulation data for volume fraction and temperature, respectively.

750 **Figure A2: Relative error of H_2O volume fraction results from simulated measured data compared to peak LOS temperature for each result.**
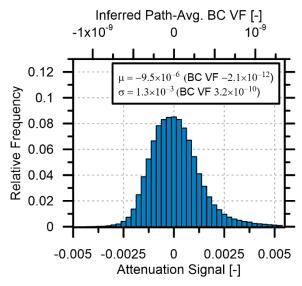
Figure A3: Light attenuation due to beam steering and inferred black carbon (BC) volume fraction (VF) presence due to the attenuation.
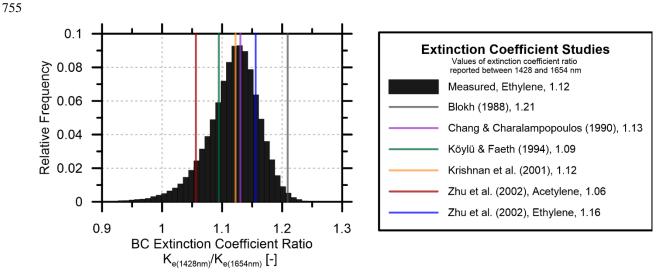
755

Figure A4: Distribution of estimated K_e ratio between 1428 and 1654 nm during ethylene flare test. The measured mean BC extinction coefficient ratio was 1.12 (standard error of the mean of 1.3×10^{-4}).

31

Table A1: Summary of black carbon extinction coefficient measurements with extinction coefficient ratios (ECRs) calculated for the wavelengths selected for measurement.

Study	Method	Fuel Source	Wavelength Range, λ [μm]	ECR [-], $K_{e_{1428}}/K_{e_{1654}}$
Blokh (1988)	Scatt/Extinction	Various	1-6	1.21[a]
Chang & Charalampopoulos (1990)	Scatt/Extinction	C_3H_6/O_2	0.4-30	1.13
Köylü & Faeth (1994)	Extinction	Various	0.2-5.2	1.09[b]
Krishnan et al., (2001)	Scatt/Extinction	Various	0.25-5.2	1.12[b]
Zhu et al. (2002)	Extinction	C_2H_2, C_2H_4	1.31, 1.56	1.06, 1.16[c]
Present Study	**Extinction**	**C_2H_4**	**1.428,1.654**	**1.12±1.3×10⁻⁴**

[a] Determined from complex index of refraction relations, assuming BC scatter-to-absorption ratio of 0.02.

[b] Calculated from interpolation of extinction data.
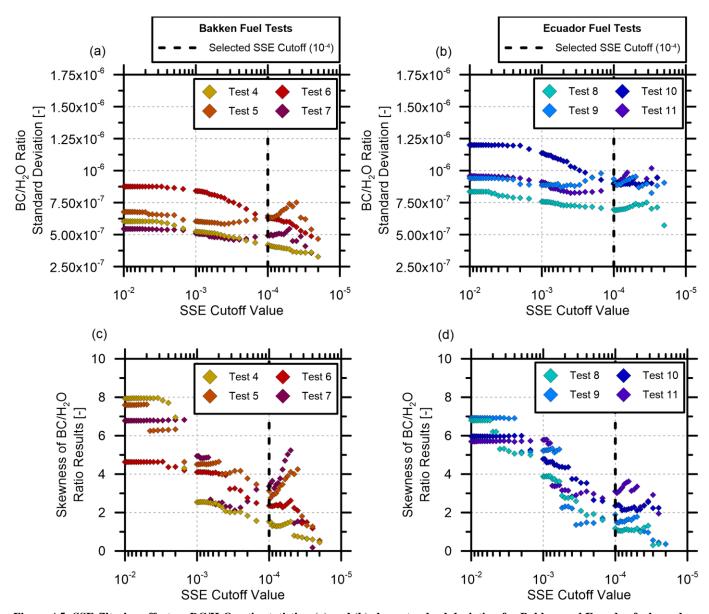
[c] BC ECR between 1565nm & 1314 nm.

Figure A5: SSE-filtering effect on BC/H$_2$O ratio statistics. (a) and (b) show standard deviation for Bakken and Ecuador fuels, and (c) and (d) indicate skewness of ratio.

Atmospheric
Measurement
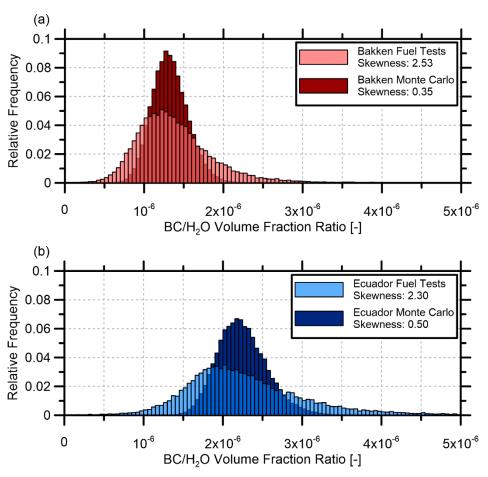Techniques

Open Access

EGU

Discussions

Figure A6: Distributions of black carbon (BC)/H$_2$O volume fraction ratios from Monte Carlo simulations with error related to beam steering, system noise, and spatial- and temporal-averaging.